ELSEVIER

Journal of Nuclear Materials 313–316 (2003) 651–656

journal of nuclear materials

www.elsevier.com/locate/jnucmat

Energy deposition and thermal effects of runaway electrons in ITER-FEAT plasma facing components ☆

G. Maddaluno [a,*], G. Maruccia [b], M. Merola [c], S. Rollet [a]

[a] *Associazione EURATOM-ENEA sulla Fusione, Centro Ricerche Frascati, Via Enrico Fermi 45, C.P. 65, I-00044 Frascati, Rome, Italy*

[b] *G & G Enterprise, Ugento (Le), Italy*

[c] *EFDA c/o Max-Planck-Institut fuer Plasmaphysik Boltzmannstr. 2, D-85748 Garching, Germany*

Abstract

The profile of energy deposited by runaway electrons (RAEs) of 10 or 50 MeV in International Thermonuclear Experimental Reactor-Fusion Energy Advanced Tokamak (ITER-FEAT) plasma facing components (PFCs) and the subsequent temperature pattern have been calculated by using the Monte Carlo code FLUKA and the finite element heat conduction code ANSYS. The RAE energy deposition density was assumed to be 50 MJ/m^2 and both 10 and 100 ms deposition times were considered. Five different configurations of PFCs were investigated: primary first wall armoured with Be, with and without protecting CFC poloidal limiters, both port limiter first wall options (Be flat tile and CFC monoblock), divertor baffle first wall, armoured with W. The analysis has outlined that for all the configurations but one (port limiter with Be flat tile) the heat sink and the cooling tube beneath the armour are well protected for both RAE energies and for both energy deposition times. On the other hand large melting (W, Be) or sublimation (C) of the surface layer occurs, eventually affecting the PFCs lifetime.

PACS: 52.40.Hf

Keywords: Runaway electrons; Energy deposition; FLUKA code; Plasma facing components; ITER FEAT

1. Introduction

The damage of plasma facing components (PFCs) by the impact of high energy runaway electrons (RAEs) [1–5] is of major concern for the design of the International Thermonuclear Experimental Reactor-Fusion Energy Advanced Tokamak (ITER-FEAT). Particularly dangerous are the RAEs generated at the end of the thermal quench of a plasma disruption. The large plasma loop voltage inductively sustained by the collapsing poloidal magnetic field can accelerate these electrons up to very high energies. The RAE energy can be eventually deposited inside the PFC material in a time-scale up to an hundred milliseconds. The main scope of this work is therefore the computing of the volumetric energy deposition and of the resulting temperature pattern in the PFCs of ITER-FEAT, for different geometries and loading conditions.

In Section 2 the different PFC configurations are reported together with the loading conditions. In Section 3 the numerical codes used for the evaluation of the energy deposition profile (FLUKA) and of the temperature pattern (ANSYS) are briefly introduced. Finally, in Section 4, the results from FLUKA and ANSYS are presented and discussed.

2. PFCs configuration and loading conditions

The volumetric energy deposition by RAEs in the PFCs and the resulting thermal field was investigated for

☆ Work supported by EFDA under contract 00-520.

* Corresponding author. Tel.: +39-06 9400 5695; fax: +39-06 9400 5314.

E-mail address: maddaluno@frascati.enea.it (G. Maddaluno).

0022-3115/03/$ - see front matter
PII: S0022-3115(02)01575-1

the following geometries: (1) primary first wall without poloidal limiters, (2) primary first wall with CFC poloidal limiters, (3) port limiter first wall (beryllium flat tile option), (4) port limiter first wall (CFC monoblock option), (5) divertor baffle first wall.

In Table 1 the material and thickness of the armour and of the heat sink as well as the material, internal diameter and pitch of the cooling tubes, are reported for all the considered geometries.

As far as the geometry 2 is concerned, a set of 18 radiatively cooled poloidal guard limiters, with circular profile, is envisaged to protect the primary first wall against the RAEs. The limiters are connected to the first wall only through a narrow stainless steel stem.

During the plasma start-up and shutdown phases, the port limiter has the specific functions of defining the plasma boundary and protecting the other regions of the primary first wall and the antennas from the direct contact with plasma.

The baffle component has the function of preventing back diffusion of particles from the divertor region. The baffle first wall is integrated in the upper part of the divertor vertical target. For all the geometries the coolant is assumed to be water, with temperature, pressure and velocity 100 °C, 3 MPa and 10 m/s, respectively.

Two electron energies, 10 and 50 MeV, were considered; RAEs were assumed to impinge on PFCs with an incidence angle of 1°, the same of the magnetic field lines. In order not to neglect the energy load by reflected electron returning on the surface, a toroidally uniform distribution of RAEs [5] and constant conditions in the poloidal direction were assumed for the simulated first wall region. The unavoidable toroidal peaking owing to first wall misalignment was successively taken into account in the choice of the surface energy density value for thermal analysis. The value of the toroidal magnetic field was assumed to be $B_T = 8$ T for geometries 1, 2, 5 and $B_T = 5$ T for geometries 3, 4, depending on the inboard or outboard location of the PFCs.

Regarding the situation just before the onset of RAEs generation, a plasma load in normal operating conditions of 0.5, 3 and 8 MW/m^2 was assumed for the primary first wall, the divertor baffle and the port limiter, respectively. A neutronic volumetric heat deposition of 5 MW/m^3 for Be and C armour and of 8 MW/m^3 for copper alloy and steel were assumed too.

3. Computational tools

The Monte Carlo code FLUKA [6] was used to compute the energy deposition profile inside the PFCs. FLUKA is an integrated, versatile multi-particle Monte Carlo program, capable to handle a wide variety of particle and radiation transport problems. With respect to previously used Monte Carlo codes, that needed an accurate choice of the step length in order to simulate in a proper way multiple scattering processes [3], FLUKA code uses a special multiple Coulomb scattering algorithm [7] making results practically independent of step size, even when thin layers or magnetic fields are present.

In this application to RAEs energy deposition, the geometrical model consists of a 3-D layered structure with the X-, Y- and Z-axis oriented along the toroidal, the poloidal and the radial direction, respectively. The structure is divided into 24 unit regions centred on the cooling tubes. Starting from the plasma, each one consists of armour, heat sink, cooling tube and coolant. Constant conditions being assumed in the poloidal direction, the patterns of electron and photon fluxes and

Table 1
The fraction of energy deposited by a RAE of 10 and 50 MeV in ITER-FEAT PFCs

Geometry	Armour material (thickness)	Heat sink material (thickness)	Cooling tube material (Φ_{int}, pitch)	RAE energy (MeV)	FW (%)	HS (%)	Tube (%)	Total (%)	Missing (%)
1	Be (10)	Cu (22)	SS (10, 28)	10	97.4	0.85	0.038	98.3	1.7
				50	84.4	6.6	0.2	92.6	7.4
2	Be/C (6/40)	Cu (22)	Cu (10, 28)	10		Limiter 96.9		97.6	2.4
				50		Limiter 86.4		88	12
3	Be (4)	Cu (23)	Cu (15, 21)	10	90.1	7.8	0.17	98.1	1.9
				50	51	33.5	2.3	88	12
4	C (15)	C (20)	Cu (10, 23)	10	96.8	0.3	0.17	97.3	2.7
				50	83.4	2.1	1.1	87	13
5	W (10)	Cu (22)	Cu (10, 23)	10	87	1.9	0.17	89	11
				50	77.1	3	0.25	80.5	19.5

In the first four columns the type of geometry, the material and thickness of armour and heat sink and the material, inner diameter and pitch of cooling tubes are reported too. Dimensions are in 10^{-3} m.

of the deposited energy were mapped in the ZX plane and radial profiles of the above quantities were produced as well.

The energy deposition was calculated both component by component (armour, heat sink, tube wall, cooling fluid), to verify the energy balance fulfilling, and with geometry binning option, by subdividing the geometry into a spatial grid based on Cartesian axes. The dimension of the bins was 0.001, 0.001 and 0.02 m in the toroidal, radial and poloidal direction, respectively. To attain a good statistics as many as 2×10^5 test particles were run.

The thermal analysis was then carried out on the basis of the volumetric energy deposition calculated in a zone fulfilling the assumption of toroidal uniformity of the RAE loading (see next paragraph).

To get the temperature pattern and the molten layer thickness (for metallic armour) in the chosen unit region the finite element heat conduction code ANSYS [8] was used.

The thickness of the mesh elements and the time step were chosen taking into account the stability constraint to be satisfied by an explicit solution method.

The steady state thermal field resulting from the normal operating conditions was firstly evaluated. Then the volumetric energy deposition values, as outgoing from FLUKA analysis, were used as input for the thermal transient analysis, for all the RAE energies and deposition times. Taking into account toroidal and poloidal peaking factors, a conservative value of 50 MJ/m^2 for geometry 1, 3, 4, 5 and 300 MJ/m^2 for geometry 2 in the time of 0.01 or 0.1 s was assumed for the energy density loading.

4. Results and discussion

4.1. Energy deposition profile

As said in Section 2, one of the input assumptions to be fulfilled is the toroidal uniformity of the RAEs energy loading. This means that 'edge effects' related to a finite size of the electron beam in the toroidal direction, are to be avoided in the numerical simulation. In other words, a suitable toroidal beam size must be chosen in order to avoid underestimating the energy deposition by disregarding the reflected RAEs returning on the surface. Therefore larger and larger toroidal dimension of the electron beam was tested, the goal being the attainment of a sufficiently large model region on which the specific energy load become independent on the toroidal dimension of the beam. From the analysis of forward and backward energy crossing the surface as well as of the deposited energy inside the PFCs it could be concluded that, for a beam toroidal length of 0.4 m, a suitable structure zone, as large as several unit regions, fulfilled the assumption of uniform toroidal distribution of RAEs. The poloidal spreading of the deposited energy outside the 0.1 m wide (in the poloidal direction) impact zone was confirmed to be negligible.

Before coming to the deposited energy patterns, it is interesting to look at the electron and photon fluences as calculated by FLUKA. In Fig. 1, as an example, these fluences (in part/cm^2) are mapped in the ZX plane for geometry 5 and electron energy $E = 10$ MeV. The direction of incident RAE beam, centred at $x = 0.2$ m, is indicated by the arrow. Due to the very shallow incidence angle, the electrons do not penetrate deeply in the wall, but are 'stopped' close to the surface: their fluence decreases very steeply moving from the surface to the first wall-heat sink boundary. The armour material influences the electron penetration and the photon production by Bremsstrahlung. For beryllium and carbon the decrease rate in the first millimeters is slower with respect to tungsten. As a matter of the fact both the main electron energy loss processes in the material at the considered energies, ionisation and Bremsstrahlung, depend on atomic number (ionisation on Z, Bremsstrahlung on Z^2). Moreover the electron energies considered in the FLUKA simulations lay well below the critical energy E_c for beryllium (namely the energy at which ionisation and radiation losses are equal). On the contrary the E_c value for tungsten is about 11 MeV [9]. Therefore a larger number of photons is to be expected for geometry 5. Bremsstrahlung photons are emitted mainly in the forward direction, because of the very shallow incident angle of RAEs. This explains the larger fraction of lost energy in the overall energy balance for geometry 5 (see Table 1). The photon fluence radial decrease is less strong of the electron one, as a result of the larger photon 'radiation length' (i.e. the length at which the fluence is reduced by a factor $1/e$) with respect to the electron one.

The pattern of deposited energy density (in GeV/cm^3) for 10 MeV incident electron energy is shown for geometry 1 in Fig. 2. In order to get a better resolution, only the magnified pattern between 0.2 and 0.5 m is shown. In Fig. 3 the energy deposited in the first wall and in the walls of the cooling tubes by 10 and 50 MeV RAEs is plotted against the region number (i.e. the toroidal dimension) for geometry 1 and 5. The integral of each curve gives the fraction of energy deposited in the corresponding component.

The fraction of the total energy per electron in each component (FW, heat sink and cooling tube) is summarised in Table 1 for all the considered cases.

As far as the energy balance is concerned, Table 1 shows that the amount of energy not accounted for increases with the atomic number of armour material and with the RAE energy. The maximum amount of missing energy (about 20% of the impinging energy) is found for geometry 5 (W armour) and $E_{RAE} = 50$ MeV. This is the

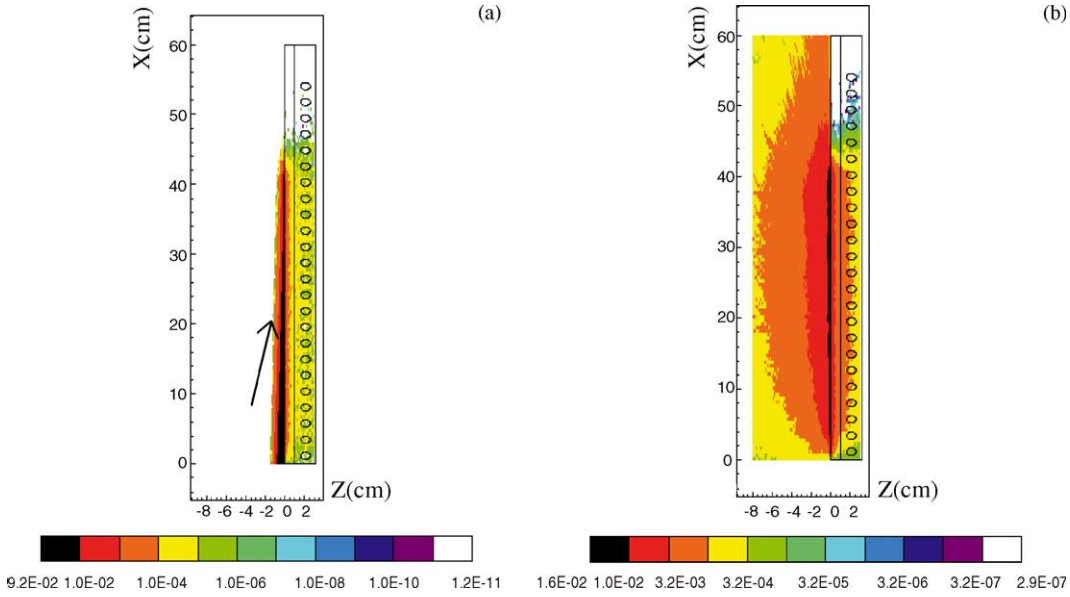

Fig. 1. Electron (a) and photon (b) fluence (cm^{-2}) in the ZX plane for geometry 5, $E = 10$ MeV. The direction of RAE incidence is indicated by the arrow in (a) (the represented incidence angle is larger than 1° for a better view).

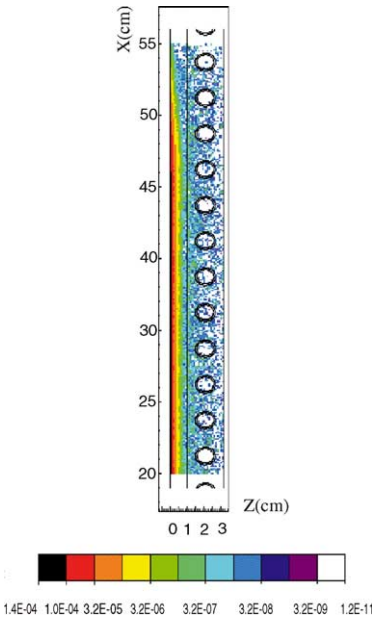

Fig. 2. Deposited energy density (GeV/cm^3) in the ZX plane of geometry 1 by a 10 MeV RAE.

result of a large photon production and probably of a large fraction of electrons reflected outside the investigated field. A very small fraction of incident energy appears to be deposited in the cooling tube walls (2.3% at most for the geometry 3, for which the armour thickness is the thinnest, and $E_{RAE} = 50$ MeV). The fraction of energy deposited in the Cu heat sink is consistent (about 33%) for geometry 3. Rather surprisingly, the fraction of energy deposited inside the cooling tube walls is larger for geometry 5 than for geometry 1, irrespective of the much larger stopping power of W with respect to Be. In principle, the comparison is not correct, the tube wall material being different; nevertheless the result, at least partially, comes from the larger photon production in W and the consequent electromagnetic shower with electron–positron pair production deeply in the structure.

4.2. Temperature pattern and PFCs damage

The pattern of the volumetric energy deposition calculated by FLUKA was used as input for the ANSYS code. The thermal analysis was carried out for one region only, chosen between the ones fulfilling the requirement of heat load toroidal uniformity. In Fig. 4, the temperature field just after the RAE energy deposition, for electron energy of 10 MeV and energy deposition time of 0.1 s, is shown for geometry 1; in this figure the amount of armour material attaining a temperature larger than the melting one, is indicated by the grey colour. Before summarising the results of thermal analysis, we remind that the melting of metallic armour material is taken into account, but no loss of material, by evaporation or removal by electromagnetic forces, is allowed. A more detailed calculation of the temperature pattern should provide for a movable boundary at the surface, in order to take into account the removal of evaporated or sublimated material.

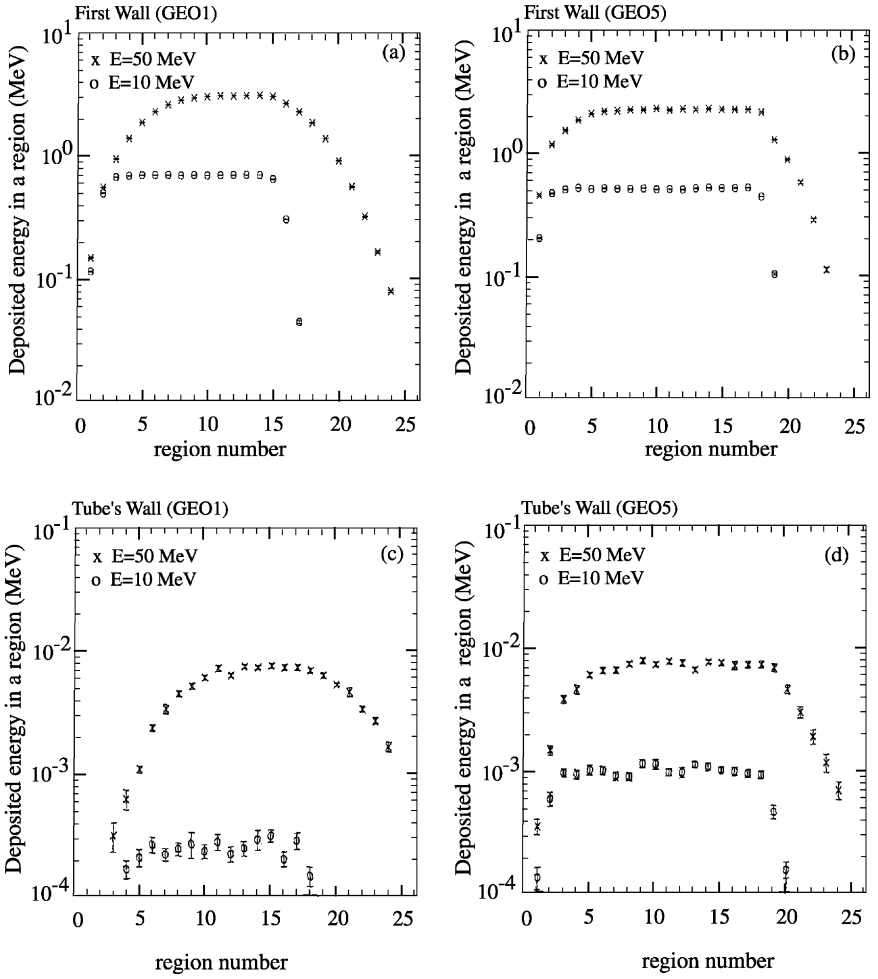

Fig. 3. Energy deposited in the first wall (a,b) and in the tube wall (c,d) regions of geometry 1 and 5 by 10 and 50 MeV RAEs.

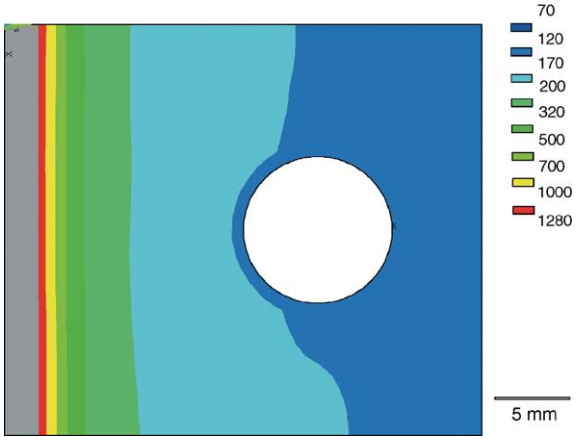

Fig. 4. Temperature pattern (in °C) for geometry 1, just after the energy deposition by 10 MeV RAEs (deposition time = 0.1 s). The grey zone indicates material attaining temperature larger than the Be melting point.

The main results of the thermal analysis are the following: the melting of armour material occurs for both geometry 1 and 3 (Be) and for geometry 5 (W). The thickness of molten beryllium can be as large as 2.5 mm for $E_{RAE} = 10$ MeV for both geometry 1 and 3. In geometry 1 molten thickness is larger for the longer energy deposition time, as expected. On the other hand no difference in the molten thickness is found for geometry 3 between 0.01 and 0.1 s energy deposition time, probably because of the thin layer of Be and the presence of Cu beneath.

For both geometry 1 and 3 the molten thickness is smaller for $E_{RAE} = 50$ MeV, because of the deeper penetration of deposited energy. The fraction of energy deposited in the armour of geometry 3 for $E_{RAE} = 50$ MeV is about one half of the one deposited for $E_{RAE} = 10$ MeV. In this case large melting of the copper heat sink occurs too. Accordingly, the maximum molten

thickness (about 1.6 mm) of W in geometry 5 is for $E_{RAE} = 10$ MeV and 0.1 s energy deposition time.

As far as the CFC monoblock geometry is concerned, the layer of material attaining temperatures larger than the carbon sublimation temperature is as thick as 1.8 mm, for $E_{RAE} = 10$ MeV and 0.1 s energy deposition time.

The temperature of the tube walls remains always well below the melting temperature of stainless steel (geometry 1) and of copper (other geometries).

The outer temperature of the tube's wall is about the same for the geometry 1 and 5, irrespective of the tungsten being a much better 'electron stopper' with respect to beryllium. As noted in Section 4.1, this results from the large photon production in W and the consequent electromagnetic shower.

As far as the geometry 2 is concerned, the high thermal load, resulting from the not full toroidal structure of the limiters, leads to an unacceptable erosion of the limiter heads: a carbon layer as thick as 13 mm attains temperatures higher than the sublimation one (and therefore is to be considered eroded), for $E_{RAE} = 50$ MeV and a deposition time of 0.1 s. On the other hand, at least within the used approximation of a merely radiative thermal coupling between the armour and the heat sink, the cooling tubes are well protected by the large mass of the carbon limiters.

References

[1] H. Calen, A. Mortsell, Uppsala University, NET Report 88-155.
[2] T. Kunugi et al., Fusion Technol. 21 (1992) 1868.
[3] H.-W. Bartels, T. Kunugi, A.J. Russo, Nucl. Fusion 5 (1994) 225.
[4] ITER Physics Basis, Chapter 3, Section 4.4.4, Nucl. Fusion 39 (1999) 2351.
[5] V. Lukash, ITER Physics Design Group at RRC 'Kurchatov Institute', Runaway Electrons and Halo Currents in FEAT Plasma, Moscow, January 2000.
[6] A. Fassò, A. Ferrari, J. Ranft, P.R. Sala, in: Proc. IV Int. Conf. on Calorimetry in High Energy Physics, La Biodola (Isola d' Elba), 20–25 September 1993, p. 493.
[7] A. Ferrari, P.R. Sala, R. Guaraldi, F. Padoani, Nucl. Instrum. and Meth. 71 (1992) 412.
[8] ANSYS User's Manual, Swanson Analysis Systems, 1992.
[9] Landolt Börnstein, Numerical Data and Functional Relationships in Science and Technology – Group I: Nuclear and Particle Physics, vol. 11, Shielding Against High Energy Radiation, Springer-Verlag, 1990.